Investigation of Blunt Bodies with CO_2 Test Gas including Catalytic Effects

Matthew MacLean[*] , Timothy Wadhams[†], and Michael Holden[‡]
Calspan-UB Research Center (CUBRC), Buffalo, NY, 14225

and

Brian R. Hollis[§]
NASA Langley Research Center, Hampton, VA, 23681

The capability to test blunt bodies using a carbon dioxide test gas with applications appropriate for Martian atmospheric reentry vehicles has been demonstrated for the LENS I facility at Calspan-UB Research Center (CUBRC). The facility was extensively calibrated at conditions of nominally 5 MJ/kg and 10 MJ/kg increased total enthalpy over a range of Reynolds numbers. This capability was used to test a 70^O sphere-cone geometry for the Mars Science Laboratory (MSL) mission, primarily to assess laminar, transitional, and turbulent heating levels as well as leeward transition criteria. The 61 cm (24 inch) diameter model was studied at 0^O, 11^O, and 16^O angles of attack. Numerical predictions of the laminar heating levels on the model were found to be inadequate without the inclusion of wall catalytic heating induced by 100% CO_2 recombination at the surface of the stainless steel model.

Nomenclature

b_{0M}	=	non-ideal correction factor	u,U	=	velocity
c	=	species mass fraction	W	=	incident shock speed
h	=	enthalpy	ρ	=	density
M	=	Mach number	α	=	angle of attack
P	=	pressure	*subscripts*		
$\tilde{R}$	=	mixture effective gas constant	s	=	adsorbed site state
Re	=	Reynolds number	0	=	reservoir or stagnation quantity
St	=	Stanton number	1	=	upstream of shock state
T	=	temperature	2	=	post-incident shock state
T_V	=	vibrational temperature			

I. Introduction

THE exploration of Mars requires reliable payload delivery systems capable of safely protecting the lander during the descent through the Martian atmosphere. Unlike Earth, the Martian atmosphere is made up of about 95.7% carbon dioxide along with other trace chemicals[1]. The nature of the carbon dioxide molecule is such that the vibrational internal energy mode is much more significant at moderate temperatures than for either nitrogen or oxygen molecules. Also, the equilibrium dissociated state of carbon dioxide is heavily temperature dependent and the large negative heats of formation of carbon dioxide and carbon monoxide cause significant net chemical energy in a dissociated shock layer behind a blunt body shock for example. The chemical and vibrational energy cause the gas to show more significant "real-gas effects" than is typically seen in air at similar energy levels. Carbon dioxide

[*] Senior Research Scientist, AIAA Member.
[†] Research Scientist, AIAA Member.
[‡] Program Manager, AIAA Fellow.
[§] Aerospace Engineer, Aerothermodynamics Branch, AIAA Senior Member.

gas also creates potentially large levels of catalytic surface heating and a sufficiently high energy gas can cause significant radiative heating from the shock layer as well.

The study of a hypersonic blunt body in carbon dioxide therefore requires a detailed accounting of these effects in order to correctly predict the heating loads of the vehicle. Testing at correctly duplicated enthalpy levels is particularly important for this type of flow because the vibrational, chemical, and radiative energies found in the shock layer are strongly dependent on the flow energy. Because numerical prediction tools require validation via experimental measurements for this type of flow, the LENS-I reflected shock tunnel facility has been used to study the heating loads on a 70^O sphere-cone as part of the preparation for the Mars Science Laboratory (MSL) mission which is set to launch in 2009.

A. Program Background and Overview

The primary objective of the LENS program with regard to the MSL mission was to study the behavior of flow transition on the forebody of the aeroshell. Although the 70^O sphere-cone geometry is quite similar to previous missions to Mars such as Viking, Pathfinder, and Mars Exporation Rovers (MER), the MSL design is significantly larger than any previous effort and the trajectory will feature a more aggressive entry velocity. Because of these facts, the flow over the vehicle will experience turbulent heating levels for much of the flight. Such heating augmentation over the laminar level requires a deeper understanding to assess its impact on the design. Besides the primary objective, the LENS tests at CUBRC also included study of the wake of the MSL design as part of an exploratory program for future work.

To accomplish these tasks, a series of 13 experiments were conducted using CO_2 test gas in the LENS-I facility for a 61 cm (24") diameter (13% full-scale) model size. Angles of attack of 0^O, the nominal flight angle of 11^O, and 16^O were studied. Most of these runs were performed using 100% Helium as a driver gas, producing relative enthalpy levels of nominally 5 MJ/kg. Two different throat inserts – a 4.1 cm (1.6") and a 2.9 cm (1.125") diameter – were used with driver pressures ranging from approximately 34.5 MPa (5,000 psia) to approximately 103.5 MPa (15,000 psia) in order to produce a series of varying Reynolds numbers for the vehicle. A single MSL run and several calibration runs were also performed using 100% hydrogen gas a driver. This condition produced nominally 10 MJ/kg of relative enthalpy.

The assessment of the transition behavior of the MSL vehicle was part of a more extensive, multiple facility program that included testing in the NASA LaRC 20-inch Mach 6 tunnel and the GALCIT T5 tunnel. A description of those phases of the program and comparative measurements can be found in Hollis, et al.[2] and Wright, et al.[3] respectively.

B. Facility Background and Overview

General hypervelocity testing at CUBRC utilizes several facilities. Currently, CUBRC operates the 48" reflected shock tunnel, the LENS-I and LENS-II reflected shock tunnels[4], and the LENS-X expansion tunnel[5]. Although any of these facilities could be used to test a model in carbon dioxide gas, the LENS-I facility was chosen as the best match to the program needs. A schematic of LENS-I and LENS-II with basic length scales is given in Fig. 1. The reflected shock tunnel uses a transient effect of an unsteady shock wave to heat a stagnant test gas to very high enthalpy levels for a short duration of time. This test gas may then be expanded through a converging-diverging nozzle in a manner similar to a blowdown facility to produce a hypervelocity test flow.

The LENS-I facility was developed primarily to study the full-scale, hypervelocity flow physics of interceptors and air-breathing engine configurations. The scale and flow duplication capabilities of LENS are such that these vehicles can be studied at their full scale, inclusive of effects such as transition to turbulence, turbulent mixing from cross-flow jets and thrusters, duplicated flow chemistry and other effects that are difficult or impossible to simulate at cold-flow or sub-scale conditions. Besides aerothermal measurements, extensive

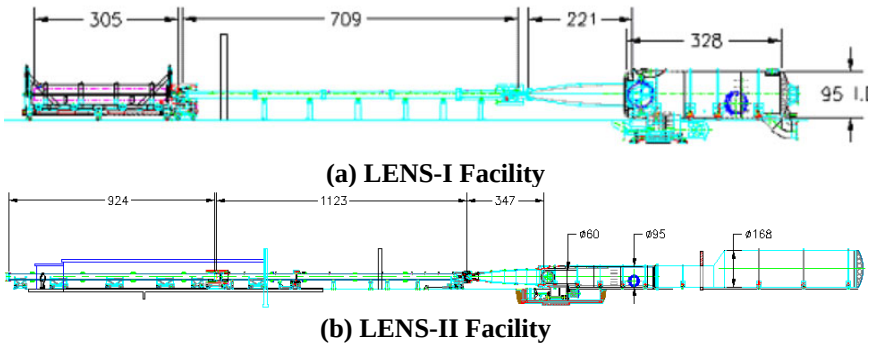

(a) LENS-I Facility

(b) LENS-II Facility

Figure 1. Drawings of CUBRC LENS Hypervelocity Reflected Shock Tunnel Facilities with Nominal Dimensions [all values shown in inches].

studies in this facility have been made using non-intruisive diagnostics such as aero-optic and aero-acoustic measurements. The capabilities of LENS-I are such that the flight conditions of interceptors and scramjet engines are fully duplicated from Mach 7 to 14, while the LENS-II facility complements it in such a way that this capability is extended down to Mach 3.5.

LENS-I was designed to be used for high-altitude, high Mach number testing. Any mixture of N_2, He, and H_2 gases can be used as a driver gas to achieve tailoring for a given condition. The low molecular weight of the hydrogen driver gas allows the LENS-I facility to be tailored to produce freestream velocities of up to 4.3 km/s (14,000 ft/s). Driver pressure can be up to 600 MPa (30,000 psia). The observed reservoir pressure during the steady-state test period in the shock tunnel will be some fractional recovery factor times this driver pressure. For the driven (or test) gas, N_2, Air, and CO_2 have been used. The current compliment of nozzles covers a range from approximately Mach 7 to 18. The equivalent altitude in air that can be simulated in LENS-I ranges from 10 to 100 km (6 to 62 mi) depending on the Mach number and other conditions. A summary of the capability range of the LENS facilities using air test gas is given in Fig. 2. As experimentation with carbon dioxide is relatively new with the LENS facilities, a similar capability range study for CO_2 is not yet available.

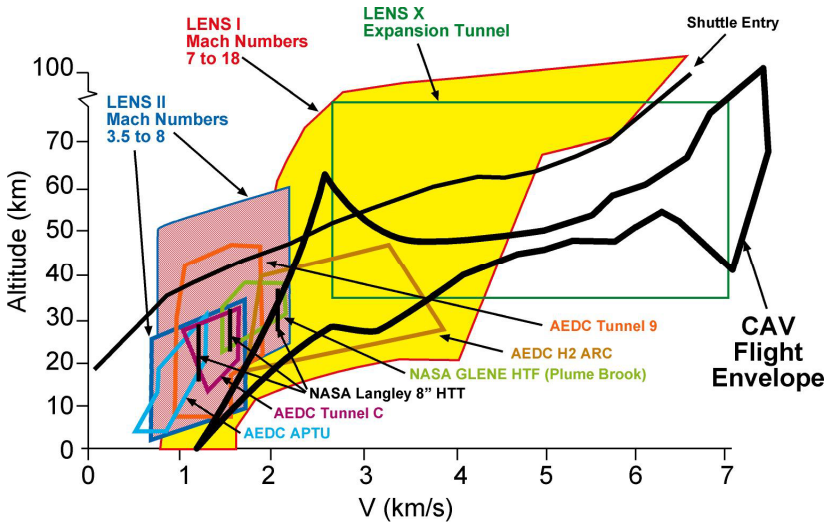

Figure 2. Velocity-Altitude Map of the CUBRC Facilities using Air as a Test Gas

II. Determination of Facility Test Conditions with CO_2 Test Gas

A. Tailoring of the Facility

The LENS-I reflected shock tunnel operates as a tailored facility, meaning that the driver/driven interface is brought exactly to a halt by the reflected shock. Operating the facility in this manner maximizes the test time available for the run, as the steady reservoir duration is limited by the arrival of the first expansion wave from the driver. In order to properly tailor the facility for a carbon dioxide test gas, a one-dimensional, inviscid method of characteristics code was used. One of the advantages of the size of the LENS tunnels is that the shocktube is of sufficient diameter that it does have a large inviscid core and the unsteady shock motion is not dominated by viscous effects. In general, it has been found that the LENS facilities agree

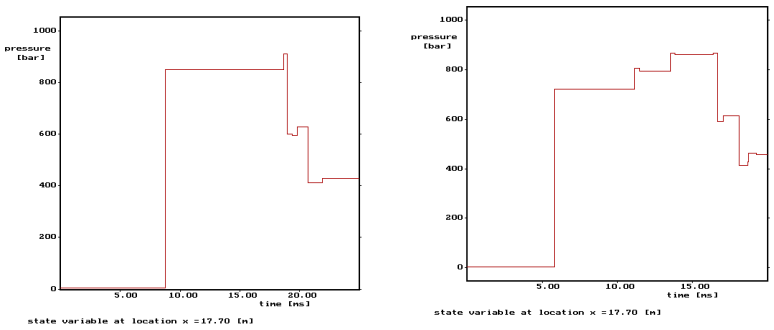

(a) helium (b) hydrogen

Figure 3. Predictions of Tailored Reservoir for LENS-I Reflected Shock Tunnel for (a) Helium and (b) Hydrogen Driver Gases

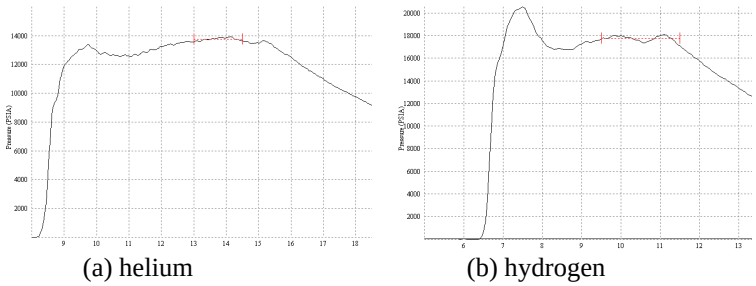

(a) helium (b) hydrogen

Figure 4. Sample Measured Reservoir Pressure Traces from LENS-I Reflected Shock Tunnel for (a) Helium and (b) Hydrogen Driver Gases

reasonably well with one-dimensional unsteady theory.

Because of the large negative heat of formation of carbon dioxide, specification of total enthalpy as a change from the initial state was found to be more intuitive. The helium driver gas was found to create nominally 5 MJ/kg of total enthalpy increase from the initial state while the hydrogen driver gas was found to create nominally 10 MJ/kg of enthalpy increase. A sample of the prediction for the tailored reservoir condition is shown for both the helium driver gas and the hydrogen driver gas is shown in Fig. 3. These predictions show that approximately 5 ms of steady state time was expected for the 10 MJ/kg cases while the 5 MJ/kg cases were expected to as much as 10 ms. Calibration of the facility resulted in about 3.5 ms of steady test time at 10 MJ/kg and about 7 ms of steady test time at 5 MJ/kg. Both conditions offer sufficient time to set up the steady-state flow over the blunt forebody of the MSL and potentially enough time to obtain wake data, particularly at 5 MJ/kg.

B. Assessment of Reservoir Conditions

Assessing the effective reservoir conditions produced by the shocktube is a critical step in the accurate prediction of the facility test conditions[6]. The reservoir of stagnant gas at the endwall of the driven portion of the shocktube is created by the passing of the incident shock which then reflects off the endwall and passes back through the test gas a second time to further increase the temperature and pressure. These reservoir conditions may be estimated in two stages by considering the motion of a single, moving, normal shock for each stage. First, the incident shock is considered, and all properties behind it are computed. The mass, momentum, and energy equations for the flow state across the incident shock are specified by Eqns. (1), (2), and (3). These are the standard jump conditions across a one-dimensional discontinuity in the coordinate system relative to the incident shock[7]. Here, the shock speed, W, is measured during the run and the initial temperature, T_1, and pressure, P_1, are recorded as part of the facility setup. Then, the reflected shock is computed in the same manner as with Eqns. (1), (2), and (3), except that the velocity is written in the coordinate system of the moving reflected shock.

$$\rho_1 W = \rho_2 (W - u_2) \tag{1}$$

$$\rho_1 W^2 + P_1 = \rho_2 (W - u_2)^2 + P_2 \tag{2}$$

$$h_1 + \frac{1}{2} W = h_2 + \frac{1}{2} (W - u_2)^2 \tag{3}$$

The equations for each shock stage contain four downstream unknowns – density, pressure, enthalpy, and either relative downstream velocity or reflected shock speed. The system of Eqns. (1), (2), and (3) (or their reflected counterparts) is closed with a suitable equation of state. The choice of this equation of state requires additional consideration.

Large densities (often more than 100 kg/m^3) can be present in the post-shock reservoir state, so the ideal gas law does not strictly apply. Instead, we have used the excluded volume correction as employed by Lordi and Mates[8] in previous work at Cornell Aeronautical Labs. In the excluded volume approach, the ideal gas law is modified to exclude the volume occupied by the gas molecules at high density. Some of the earliest work in using non-ideal gas effects for one-dimensional flows was done by Eggers[9], while Korte, et al.[10] and later Candler[11] have demonstrated the use of non-ideal gas effects for a general CFD code to compute nozzle flows. The excluded volume relation is given in Eqn. (4).

$$P = \frac{\rho \tilde{R} T}{(1 - b_{0M} \rho)} \tag{4}$$

Here, the constant b_{0M}, called the co-volume, is a term reflective of the compressibility of the gas. The value that has been used for CO_2 is 0.000975 m^3/kg, which was based on available data on the virial coefficients of carbon dioxide. This value is also consistent with the accepted value of 0.00111996 m^3/kg for air and nitrogen, as the compressibility of many common gases can be shown to be similar[12]. One can see that for small to moderate densities, the ideal gas law is approximately returned, while the excluded volume effect becomes significant only for large densities. The computed enthalpy of the gas is also modified accordingly by the excluded volume equation. The excluded volume effect was found to be particularly important in the MSL testing in LENS because some of the runs had reservoir densities in excess of 120 kg/m^3.

The mixture gas constant in the equation of state is evaluated by assuming equilibrium dissociation of the gas. The standard equilibrium constant curve fits are used from the Gordon and McBride model[13], which are functions of temperature only. Diatomic species are also assumed to have relevant vibrational modes in full equilibrium with the

translational temperature for the calculation of enthalpy. Because of the large densities in the reservoir, the relaxation times of the chemistry and vibrational states are very short. Four species were included in the calculations – CO_2, CO, O_2, and O. Atomic carbon, C, was initially included in the calculations, but was found to be irrelevant for the conditions in the LENS tests.

C. Assessment of Freestream Conditions

Using the known reservoir conditions, the flowfield of the nozzle was computed for each case using a specialized, full Navier-Stokes, structured solver for axisymmetric flows. This code is based on the data-parallel line relaxation method[14] and implements a modified (low dissipation) Steger-Warming flux splitting approach[15] for the convection terms and central differencing for the diffusion terms. Turbulence is incorporated via the Spalart-Allmaras one-equation turbulence model[16] with the Catris and Aupoix compressibility correction[17]. Finite rate chemistry is included with the four species used in the calculation of the reservoir using rate information from Park, et al[1]. Finite rate vibrational relaxation is also included via a single vibrational degree of freedom[18] using the Landau-Teller model[19]. Vibrational energy relaxation rates are computed by default from the semi-empirical expression due to Millikan and White[20], but rates from the work of Camac[21] are substituted where available for the CO_2-CO_2 collisions. The nature of this particular series of LENS tests was such that the vibrational energy was found to be very close to equilibrium for all runs, so the choice of vibrational relaxation rates did not significantly affect the outcome of the calculation (both methods were evaluated initially). The code also uses the excluded volume equation of state in its formulation. This model is particularly important for CO_2, as the excluded volume correction does affect the computed total enthalpy of the flowfield.

The estimated reservoir conditions were used as an inflow boundary condition and the wall boundary condition was assumed to be isothermal at the lab temperature. This constant wall temperature assumption is known to be valid for the short-duration test facilities at CUBRC. Using this information, the calculation of the steady-state nozzle expansion to the test section was performed for each run in both the calibration and the run sequences. Because of the speed of the solver and the computing resources available at CUBRC, these computations were completed in one hour or less for each case. Additional details concerning the computation of nozzle flowfields may be found in Ref. 6.

III. Supporting Numerical Tools

The MSL program in LENS was supported with extensive computations in addition to those used to compute the freestream conditions. While the nozzle code was used only for that particular specialized problem, the DPLR code[14] from NASA Ames Research Center was used for general model calculations in order to verify and support the data. DPLR is a multi-block, structured, finite-volume code that solves the reacting Navier-Stokes equations including finite rate chemistry and finite rate vibrational non-equilibrium effects. DPLR is distinct from the nozzle code, but the two do share a common heritage. DPLR uses the same data-parallel line relaxation scheme for steady-state time integration and modified, low dissipation Steger-Warming flux splitting approach[15]. A five species (CO_2, CO, O_2, C, O), 6-reaction model was used to compute all calibration and model flowfields for the program. Vibrational relaxation is modeled with the Landau-Teller model. Transport properties are appropriately modeled in DPLR for this type of flow[22,23] using the binary collision-integral based mixing rules from Gupta, et al[24]. Diffusion coefficients are modeled using the self-consistent effective binary diffusion (SCEBD) method[25].

Turbulence models available in the DPLR code currently include the Baldwin-Lomax 0-equation model[26] and the Shear Stress Transport (SST) 2-equation model[27]. Both options are RANS-type models. Both models are corrected for compressibility effects[28]. The Spalart-Allmaras model[16] has also been recently incorporated into the DPLR code and is currently being fully evaluated.

The issue of wall boundary condition deserves some specific consideration. The non-catalytic wall boundary condition provides the lowest level of surface heating. The super-catalytic boundary condition provides the highest possible level of heating because the mixture has been returned to its lowest possible energy state at the wall, meaning that the maximum amount of chemical energy has been returned to the other modes. In this case, that state corresponds to 100% CO_2. The super-catalytic boundary is non-physical in that it does not identify a specific mechanism by which the recombination occurs, but assumes that it has occurred by some unidentified process without consideration of rate mechanics.

The Mitcheltree wall catalysis model[29] has been used in previous Mars entry vehicle designs. In the Mitcheltree model, CO_2 production at the surface is essentially controlled by the oxidation of CO with atomic oxygen in an E-R reaction where either molecule has been adsorbed by the surface. The rate of recombination is controlled by the rate of diffusion of the molecules to the surface. Evaluation by Wright, et al.[3] showed that the Mitchtree model predicted

catalytic heating rates that were only slightly higher than the corresponding non-catalytic rates. This is largely due to the fact that, with the conditions produced in both the LENS-I and T5 facilities, the bulk of the oxygen is trapped in the form of O_2 molecules. The Mitcheltree model was generally found to be unable to predict the level of heating found in both LENS and T5.

$$( )_S + CO \Leftrightarrow (CO)_S \tag{5a}$$

$$( )_S + O_2 \Leftrightarrow (O)_S^1 + (O)_S^2 \tag{5b}$$

$$(O)_S^1 + (CO)_S \Leftrightarrow CO_2 + ( )_S \tag{5c}$$

$$(O)_S^2 + (CO)_S \Leftrightarrow CO_2 + 2( )_S \tag{5d}$$

Adequate prediction of the MSL program heating levels therefore requires a catalysis model in which molecular oxygen is used to convert CO into CO_2 at the surface. Such a mechanism was previously identified by Wright, et al. from the literature database in the automotive catalytic converter community. The work of Bonzel and Ku[30], for instance, demonstrated the catalytic reaction of CO and O_2 on a Platinum surface. Additional work from the catalytic converter community has identified similar mechanisms on other precious metals such as Palladium[31] and Ruthenium[32]. However, Wright, et al. were unaware of any work that had been done specific to steel surfaces.

Further searching of the literature has revealed that the work of Jenkins and Voisey[33] did indeed identify a catalytic effect on stainless steel. Their experimental measurements suggested that O_2 occupies a single adsorbed site on the steel surface and the oxidation of CO occurs as part of a two step L-H reaction between the adsorbed and dissociated oxygen atoms with adsorbed CO molecules. This mechanism is repeated in Eqns. (5a) – (5d). The rates of this mechanism were made on 18/8 stainless steel, but Jenkins and Voisey proposed that the results would be generally applicable to any stainless alloy. As this information is a relatively recent finding, the detailed rates of this mechanism have not been evaluated with regard to the MSL program yet. However, the identification of such a mechanism provides a plausible justification for the heating levels that have been measured in the LENS-I and T5 facilities.

IV. Calibration of the LENS-I Facility for CO_2 Test Gas

Because this program was the first to use CO_2 as a test gas in LENS-I, the facility was extensively calibrated before installing the model in order to better validate the test sequence and understand the characteristics of the flowfield and tunnel operation. Calibration runs were made at both the 5 MJ/kg and the 10 MJ/kg enthalpy levels to fully validate the test matrix. A summary of freestream conditions for all six runs comprising the calibration series is given in Table 1.

Table 1. Summary of Freestream Conditions for LENS-I Facility CO_2 Calibration Series

run	Re (1/m)	M	P (Pa)	T = T_V (K)	ρ (kg/m^3)	U (m/s)	Δh_0 (MJ/kg)	c_{CO2}	c_{CO}	c_{O2}	c_O
211	2.70E+5	6.88	706	990	3.16E-3	3,620	9.95	0.6203	0.2417	0.6701	0.6945
212	4.44E+5	6.78	1,348	1,110	5.45E-3	3,727	10.25	0.6528	0.2210	0.2100	0.1944
213	6.25E+5	6.66	2,113	1,203	7.95E-3	3,789	10.48	0.6701	0.2100	0.1160	0.1081
215	8.35E+5	6.57	3,119	1,292	1.10E-2	3,857	10.80	0.6788	0.2044	0.1131	0.0036
219	1.33E+6	6.77	2,132	712	1.54E-2	2,772	4.76	0.9390	0.0389	0.0222	0.0000
220	2.02E+6	6.22	4,713	892	2.70E-2	2,845	5.26	0.9262	0.0470	0.0268	0.0000

A. Calibration of the Facility at 10 MJ/kg

The LENS-I facility was calibrated using 100% hydrogen driver gas with four runs at driver pressures of 34.5 MPa (5,000 psia), 69.0 MPa (10,000 psia), 103.5 MPa (15,000 psia), and 138.0 MPa (20,000 psia). All four of these runs used the 2.9 cm (1.125") nozzle throat insert, which produces a Mach number of nominally 6.75 at the exit of the nozzle. In each case, the calibration sequence consisted of a rake of Pitot pressure gages across the core of the test section just downstream of the nozzle exit plane. A 6.75^O half-angle cone with a surface pressure measurement was also attached to the rake for most runs. Hemisphere probe heat transfer measurements were also available for some runs.

As an example of the nozzle flowfield computation, the measured and computed Pitot pressure profile for the rake plane is compared in Fig. 5 for run 215, the highest pressure run of the four. The calculation is shown to agree with the measurement very well. The core extends to a radius of approximately 46 cm (18") at this station, which

the numerical solution predicts correctly. Within the bulk of the core, the variations between the measurements and the calculation compare within 3.5% or less for any given gage.

The solution of the Mach number at the nozzle exit plane for this run is shown in Fig. 6. As with the Pitot pressure profile, the uniformity of the flowfield is demonstrated. In the core, Mach number is held to within +/- 0.25% at that axial station.

As mentioned, the vibrational relaxation rate of carbon dioxide is such that the flow was found to be approximately in vibrational equilibrium for all runs. The chemical recombination processes, however, were found to freeze

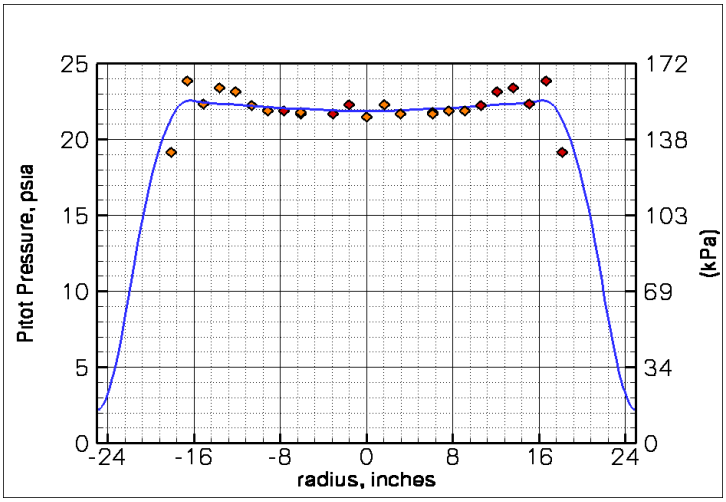

Figure 5. Pitot Pressure Profile for Run 215 and Comparison with Numerical Prediction

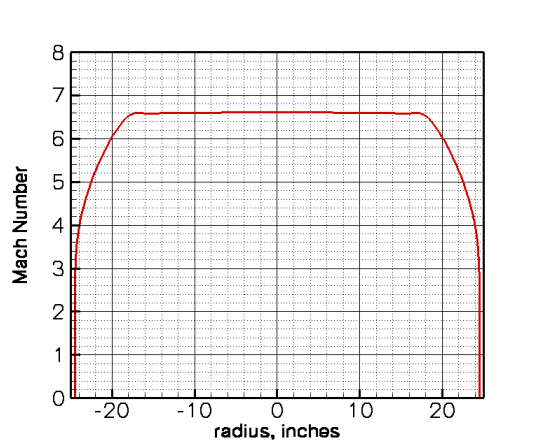

Figure 6. Predicted Mach Number Profile for Run 215 at Nozzle Exit Plane

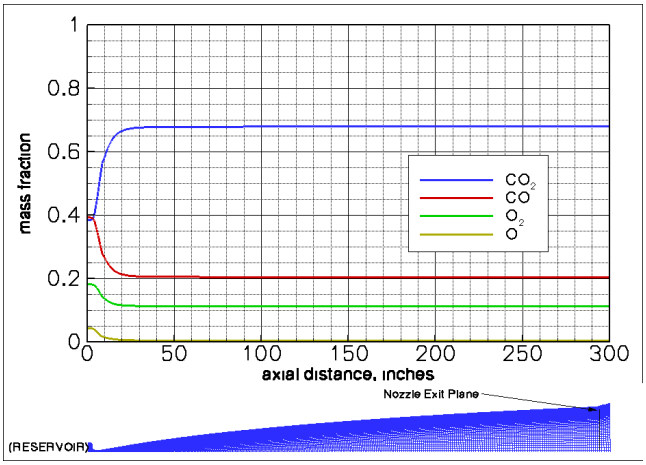

Figure 7. Species Mass Fractions for Run 215

partially through the expansion. This effect is particularly important for the 10 MJ/kg runs, as a significant portion of carbon dioxide dissociated in the reservoir, and a significant amount of flow energy was found to be trapped in residual chemical dissociation at the test section station. The mass fractions of the four species that were considered are shown in Fig. 7 for run 215. In this case, it was found that about 68% of the CO_2 had recombined with the remaining species trapped as carbon monoxide and molecular oxygen.

Besides the Pitot pressure profile, the measured heat transfer rates from the hemisphere probe are an important measure of correct calibration of the facility. For run 215, a 7.6 cm (3") diameter steel hemisphere was used with four coaxial heat transfer gages located at increasing angles around it. The solution for the 7.6 cm (3") hemisphere was

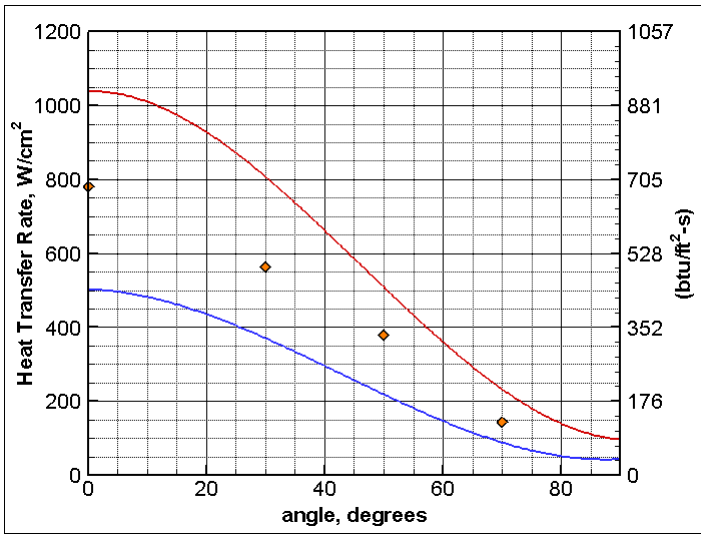

Figure 8. Comparison of Predicted and Measured Heating Levels on Three Inch Hemisphere Model for Run 215

calculated using both the non-catalytic and super-catalytic boundary conditions with the DPLR code. These results and the comparison with experiment are shown in Fig. 8. The measured heat transfer rates fall about half way between the two extreme solutions. As these two solutions provide a lower and an upper possible bound for the heating rates, the measured data is consistent with the predictions. The fact that it lies somewhere between the two bounds suggests that there is some catalytic behavior at the metal surface, but the catalysis mechanism is limited by one of the surface reactions in some way. It is unclear if this trend is indicative of the catalytic mechanism or if there are outstanding issues to consider. A smaller, 1.9 cm (0.75") diameter hemisphere with a thin-film type heat transfer gage at the stagnation point displayed a similar trend. The measured rate on the smaller hemisphere was 1,750 W/cm^2 (1,541 btu/ft^2-s), which is roughly halfway between the computed non-catalytic and super-catalytic levels of 1,007 W/cm^2 (887 btu/ft^2-s) and 2,166 W/cm^2 (1,907 btu/ft^2-s).

B. Calibration of the Facility at 5 MJ/kg

The calibration of the LENS-I facility at the 5 MJ/kg conditions was performed similarly, but using 100% helium as a driver gas. For this enthalpy level, two runs were performed. The first run (219) used the same 2.9 cm (1.125") throat and a 103.5 MPa (15,000 psia) driver pressure. The second of the two runs (220) used the 4.1 cm (1.60") throat insert. This slightly larger throat lowered the exit Mach number but raised the freestream Reynolds number by nearly a factor of two. As obtaining turbulent data was a primary objective of this program, it was determined that the bigger Reynolds number range was important. Changing the nozzle throat component was favored over raising the driver pressure above 103.5 MPa (15,000 psia) because of the wear on the facility and the model with very high driver pressures.

The Pitot pressure at the rake plane in the test section for both runs is shown in Fig. 9. Here, very good agreement with the calculations is found again. The core size and level is well-predicted, suggesting that the computed freestream conditions are reasonably accurate.

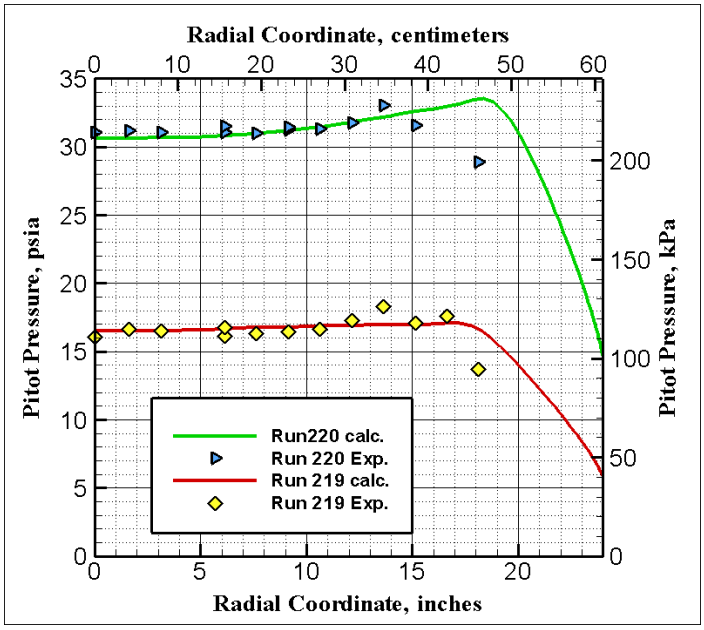

Figure 9. Pitot Pressure Profile for Runs 219 and 220 including Comparison with Numerical Predictions

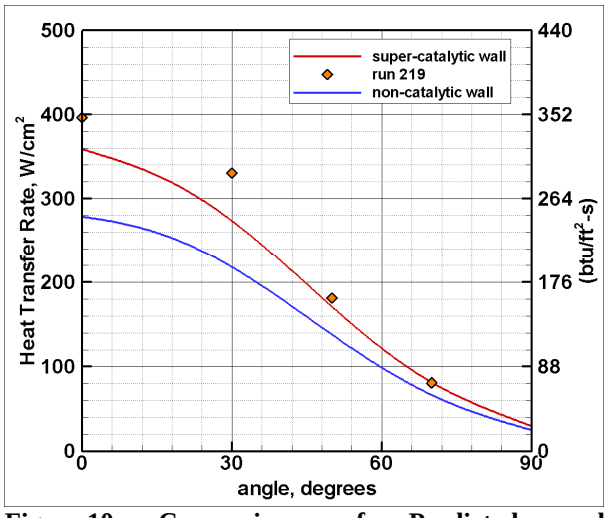

Figure 10. Comparison of Predicted and Measured Heating Levels on Three Inch Hemisphere Model for Run 219

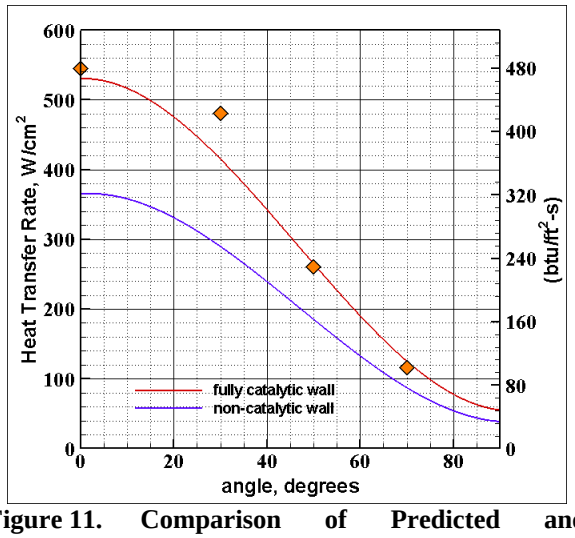

Figure 11. Comparison of Predicted and Measured Heating Levels on Three Inch Hemisphere Model for Run 220

The 4.1 cm (1.60”) throat configuration of run 220 shows a slight concavity in Pitot pressure, which is a function of some residual expansion waves that have not fully cancelled. However, in the core region, the total (peak-to-peak) variation in Pitot pressure is less than 7%, which is satisfactory. The 2.9 cm (1.125”) throat shows nearly perfect cancellation across the core for run 219.

The calculations for the 7.6 cm (3”) thin film hemisphere model and the comparisons with the measured data for these two runs are shown in Figs. 10 and 11. Here, the conclusion is somewhat different than for the 10 MJ/kg cases. For both run 219 and run 220, the experimental data matched closely with the super-catalytic wall boundary condition solution. For run 220, analysis of this solution and solutions of the thin film hemisphere models of 1.9 cm (0.75”) and 3.2 cm (1.25”) diameters, the maximum deviation between theory and experiment at the stagnation point is less than 5%. For run 219, the deviation between theory and experiment is about 8%, which is still considered to be a well-characterized condition. This suggests that virtually 100% of the CO_2 is recombining at the wall and that the mechanism for this flowfield involving O_2 is active and is not rate limited as it seemed to be in the 10 MJ/kg case.

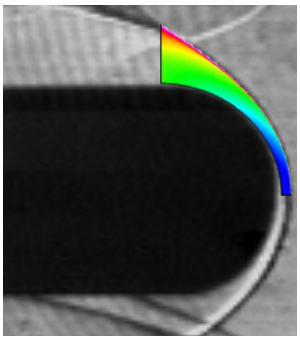

Figure 12. Comparison of Experimental Schlieren and Computed Shock Shape for Three Inch Hemisphere for Run 220

As a final check of the calibration of the flowfield quality and freestream condition accuracy, the shock pattern on the 7.6 cm (3”) hemisphere model was captured with Schlieren photography for run 220. The comparison with the predicted shock shape from the DPLR solution is shown in Fig. 12. The shock stand-off distance is a rough check that the Mach number is predicted approximately correctly for the flowfield. The possibility of helium contamination was considered here also by running the same DPLR calculation with helium gas instead of CO_2. The helium shock clearly did not match the Schlieren picture, providing a cursory check that the facility did not suffer a significant helium contamination problem.

V. Description of MSL Program

A. Model Construction

A 61 cm (24”) diameter stainless steel model of the MSL vehicle was constructed, consisting of a forebody, and aftbody, and the sting assembly. The model as it was tested is approximately 13% of the full-scale flight vehicle. Details of the geometry, complete with all relevant dimensions, are given by Hollis, et al[2]. This model was instrumented with a total of 83 thin-film heat transfer gages, 10 coaxial thermocouple heat transfer gages, and 10 pressure gages. The bulk of the instrumentation was placed along the windward and leeward centerline rays of the forebody with a smaller number

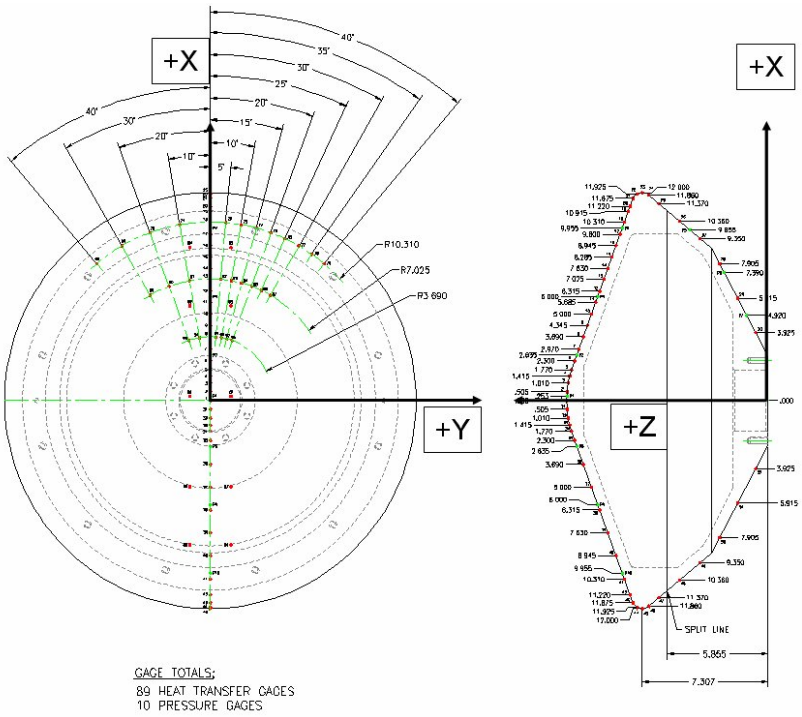

Figure 13. Gage Layout Drawing Showing Instrumentation Locations for CUBRC MSL Model

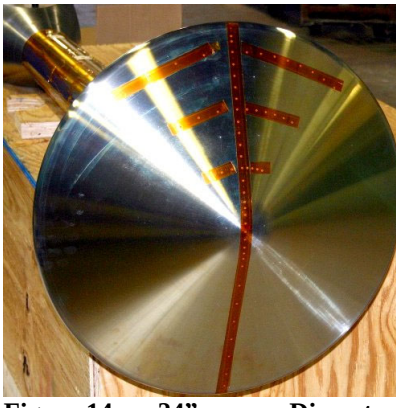

Figure 14. 24” Diameter CUBRC MSL Model with Installed Gages

of gages on the aftbody of the vehicle. Some heat transfer gages were placed off-center on the leeward side along three constant radius lines. These gages were placed to provide additional points in the expected transition region. The gage layout on the model is shown in Fig. 13. Beside those on the model surface, four heat transfer gages of the total were placed on the sting to capture heating rates in the wake of the MSL and are not shown in the figure. The model as instrumented is shown in Fig. 14.

In an effort to prevent catalytic heating effects to the model, the entire surface was coated with a magnesium fluoride (MgF_2) deposition. This is the same compound that is often used with thin-film gages to prevent catalysis on the platinum strip. During the deposition process, five of the coaxial thermocouples were coated and five were left uncoated to ascertain whether any catalytic effects occurred. As the results of the program will show, there is question whether the coating was effective on the model, as the heating rates on the forebody showed general agreement with the super-catalytic predictions. Monitoring of the magnesium fluoride coating during the program did show that the coating was eroded off the model during the test sequence, but the data seems to indicate that it was not effective in preventing catalysis from the beginning.

B. Model Installation and Run Matrix

The MSL model was installed in the LENS-I facility with the nose at a station close to the Pitot rake plane to insure that the model would be tested in a good quality flowfield. Computations of the flowfield conditions showed that the model was well within the core and that there were no large axial or radial gradients in the flow. The model as installed in the tunnel is shown in Fig. 15. The model was tested over 13 runs in the LENS-I facility at three angles of attack: 0^O, 11^O, and 16^O. These angles were chosen because 11^O is the nominal flight entry configuration in the Martian atmosphere, 16^O was selected because it was thought to provide a better chance to obtain turbulent heating data, and 0^O was chosen to because it provided axisymmetric data for easier code validation. The run matrix was divided up with 5 runs at 16^O, 5 runs dedicated to 11^O, and the remaining 3 runs at 0^O. The sting assembly was designed with spacer blocks in the base such that the model nose was located in the same position in the flowfield for all the angles of attack. Some initial concern was expressed about the large size of the model and a potential "blockage" effect caused by its presence at the end of the nozzle. As Williams[34] points out, however, the negligible back pressure in shock tunnel facilities generally allows them to sustain started flow through contractions right up to the isentropic limit. At Mach 6 in carbon dioxide, this isentropic limit is very large, nominally 300:1. Although viscous effects may decrease this limit in practice, it is the opinion of these authors that it is not possible to reduce it down to the (1.34):1 ratio of the installed MSL model. A post-program run in which

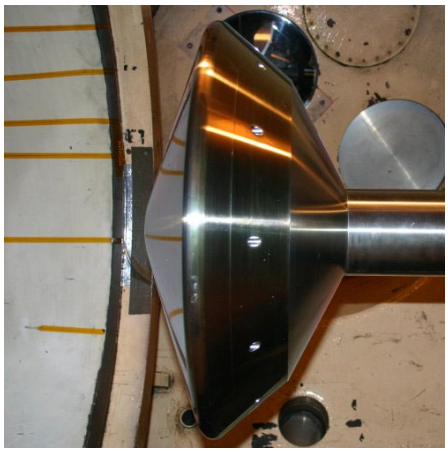

Figure 15. CUBRC MSL Model Installed in the LENS-I Facility

Table 2. Summary of Freestream Conditions for CUBRC MSL Program in LENS-I Facility

run	α (deg)	Re (1/m)	M	P (Pa)	$T = T_V$ (K)	ρ (kg/m^3)	U (m/s)	Δh_0 (MJ/kg)	c_{CO2}	c_{CO}	c_{O2}	c_O
1	16	1.18E+6	6.79	2,022	760	1.36E-2	2,880	5.12	0.9221	0.0496	0.0283	0.0000
2	16	1.94E+6	6.30	4,202	863	2.49E-2	2,833	5.06	0.9119	0.0561	0.0320	0.0000
3	16	4.56E+5	6.79	692	686	5.09E-3	2,762	4.84	0.9007	0.0632	0.0361	0.0000
4	16	9.14E+5	6.74	1,438	710	1.04E-2	2,760	4.70	0.9263	0.0469	0.0268	0.0000
5	16	6.64E+5	6.71	2,188	1,190	8.42E-3	3,769	10.20	0.6945	0.1944	0.1081	0.0030
6	11	2.11E+6	6.21	4,512	854	2.70E-2	2,777	4.88	0.9315	0.0436	0.0249	0.0000
7	11	4.75E+5	6.77	721	687	5.30E-3	2,753	4.80	0.9028	0.0619	0.0353	0.0000
8	11	1.44E+6	6.25	2,871	805	1.82E-2	2,722	4.72	0.9239	0.0484	0.0277	0.0000
9	11	7.86E+5	6.26	1,523	785	9.78E-3	2,711	4.82	0.8993	0.0641	0.0366	0.0000
10	11	8.51E+5	6.75	1,397	732	9.70E-3	2,817	4.95	0.9158	0.0536	0.0306	0.0000
11	0	2.00E+6	6.23	4,367	867	2.57E-2	2,809	5.00	0.9285	0.0455	0.0260	0.0000
12	0	4.71E+5	6.77	720	691	5.26E-3	2,761	4.84	0.9008	0.0632	0.0361	0.0000
13	0	8.30E+5	6.78	1,385	741	9.48E-3	2,849	5.07	0.9116	0.0563	0.0321	0.0000

the model was moved backward in the facility verified this assumption.

The complete run matrix for the MSL program is given in Table 2. The model was tested at each angle of attack over a large range of Reynolds number. It was decided to concentrate the runs on the 5 MJ/kg enthalpy condition, as the 10 MJ/kg condition tended to cause increased wear on both the facility and the model. Thus, only a single run was performed at 10 MJ/kg, while the rest were performed at 5 MJ/kg. The primary purpose of the test sequence was to obtain transitional data, and the enthalpy level of the flow was not evidenced to be a significant factor on transition behavior.

C. Experimental Data: Results and Validation

The results of the heating on the forebody of the MSL at 16^{O} angle of attack are shown in Fig. 16. All gages on the centerline only are shown. The heating has been non-dimensionalized using a Stanton number formulation with a factor to remove the effect of Reynolds number. Looking at the data in this way more easily shows the transition point on the model at each Reynolds number. Solutions with the DPLR code for a laminar non-catalytic wall and laminar super-catalytic wall are shown for comparison. Since the heating is dimensionless, the numerical solution from only one run is given.

Referring to Table 2, the order of runs from smallest Reynolds number to largest at this angle of attack is 3, 5, 4, 1, and 2. First, as noted by previous authors and earlier in this paper, the super-catalytic boundary condition is necessary to adequately predict the laminar heating level. This finding is consistent with the results obtained from other CFD codes and grids[2,3]. One may conclude that this behavior is possibly a result of the limited thermochemical and surface-catalytic database that is common to the numerical tools. Comparing with the laminar super-catalytic solution shows that run 3 displays laminar to transitional data over the leeward side. The fact that run 3 shows a departure from the predicted solution half-way down the leeward side suggests that the flow may have started to transition at even this low Reynolds number. The other four runs show successively earlier transition points based on the sudden elevation of heating. Run 2, at the largest Reynolds number, shows only about three gages in the laminar region at the nose. Even run 5, at the larger enthalpy level, seems to follow the trend consistently with the others. Because no completely laminar data was obtained at this largest angle of attack, planned future tests with a smaller model will establish a laminar baseline.

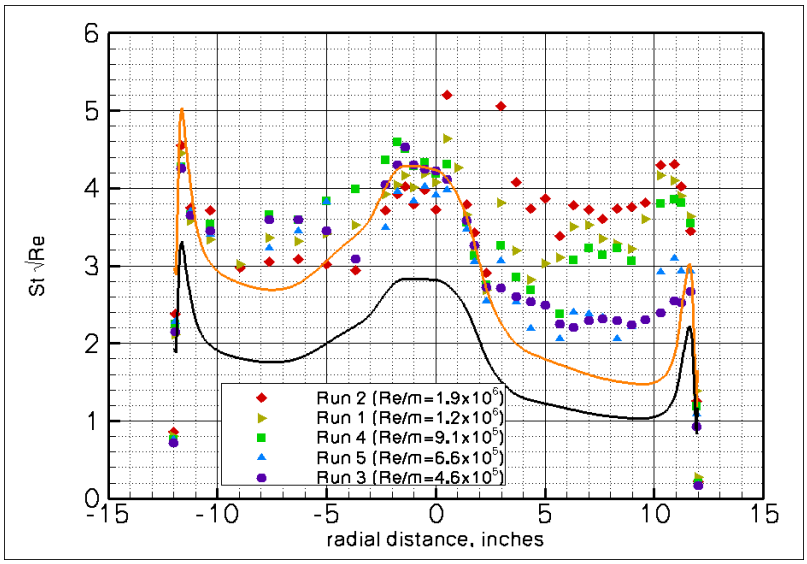

Figure 16. Non-Dimensionalized Heating Data on Centerline of MSL Forebody at 16^{O} Angle of Attack

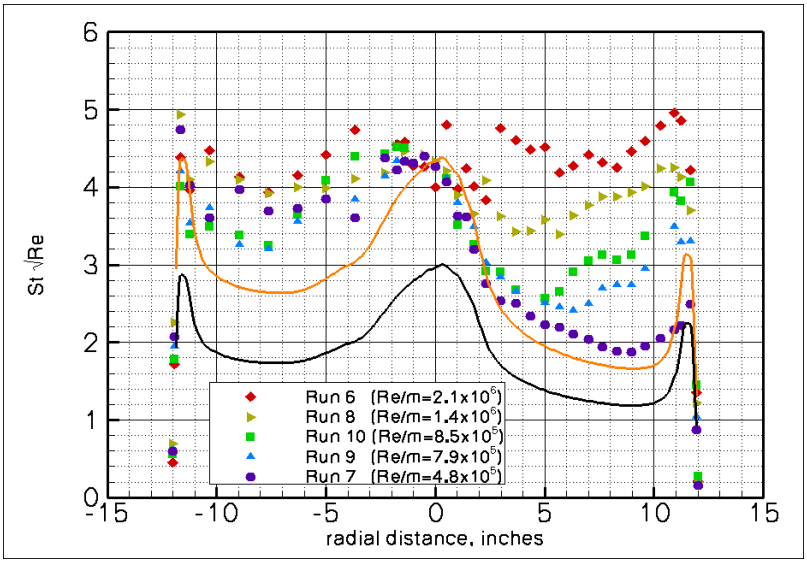

Figure 17. Non-Dimensionalized Heating Data on Centerline of MSL Forebody at 11^{O} Angle of Attack

The same comparison is shown for the five runs at an angle of attack of 11^{O} in Fig. 17. Here, the heating

comparison is similar to what it was at 16^O. One of the reasons that the 16^O configuration was tested first was because there was some initial concern that turbulent flow could not be generated at the smaller angle of attack. The large physical size of the model made this concern a non-issue, however. Here, the set of runs is 7, 9, 10, 8, and 6 in order of smallest Reynolds number to largest. Here, again, run 6 – the largest Reynolds number run – shows turbulent flow very close to the stagnation point. Run 7 – the lowest Reynolds number run – displays good agreement with the laminar, super-catalytic prediction as was the case at the higher angle of attack.

It is interesting to note that, at both 11^O and 16^O angle of attack, the windward side heating also displays some elevation over the laminar solution level starting part of the way down the face. It was unexpected to see any transition on this side of the model, and the measurements do not seem to display a definitive trend based on freestream Reynolds number. It is unclear whether this is a potential windward side transition or whether some other issue is occurring on that side of the model. There is some indication of windward heating augmentation from the LARC Mach 6 tests[2] and T5 nitrogen tests on this configuration[35], but the mechanism that causes this behavior in any of the facilities is not understood and requires further study.

Finally, the dimensionless heating data for the 0^O angle of attack runs is shown in Fig. 18. By this point in the run matrix, the attrition rate of the sensitive thin-film gages had resulted in the loss of a significant number of them, particular in the nose region. Here, it was seen that even at 0^O angle of attack, the LENS-I facility had no trouble in producing turbulent flow on the vehicle. Run 12 is the only run from the LENS MSL tests that shows fully laminar behavior over the entire model surface. The other two runs at a higher Reynolds number show transition about half-way down the body. Also, it is important to notice that the data is symmetric on the model. This is a check of the facility flowfield quality and the consistency of the instrumentation on the model. The symmetry in the measurements was seen with the transition point in the higher Reynolds number runs also.

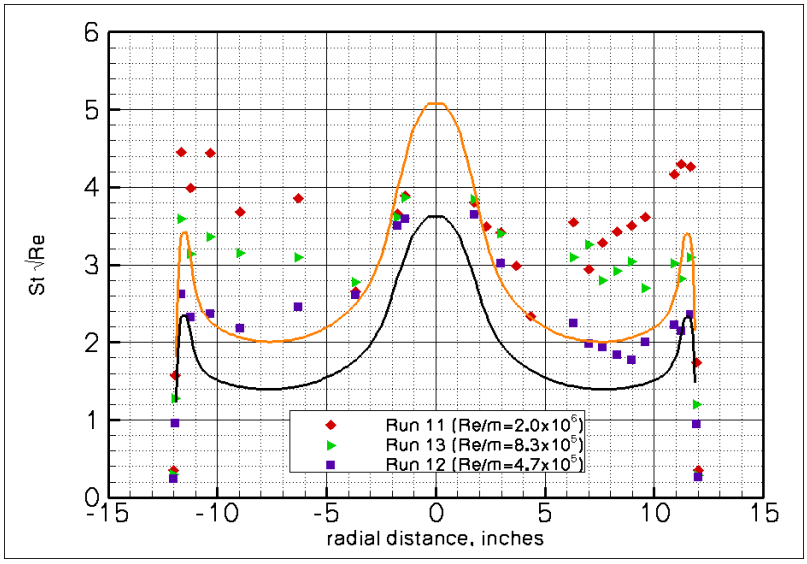

Figure 18. Non-Dimensionalized Heating Data on Centerline of MSL Forebody at 0^O Angle of Attack

Finally, run 5 is compared to the predicted non-catalytic and super-catalytic predictions. As run 5 was the only run performed at the 10 MJ/kg enthalpy condition using hydrogen driver gas, it deserves special consideration. This comparison is shown dimensionally in Fig. 19. Here, one sees that run 5 shows the transitional behavior on both the leeward and the windward rays midway down the model that was discussed previously. This run was the last in the 16^O angle of attack configuration, for which no fully laminar data was captured over the entire body. If the comparisons are analyzed more closely, however, it seems apparent that the super-catalytic solution over-predicts the heating near the stagnation region, where the flow

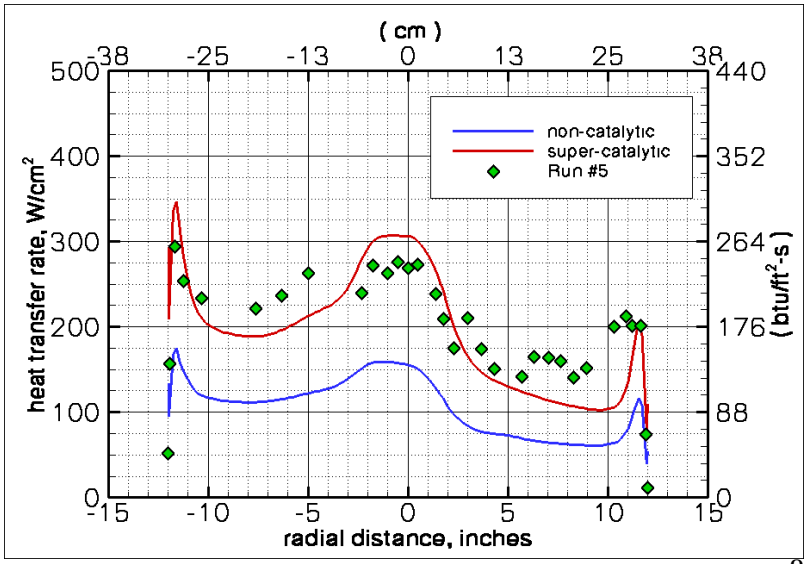

Figure 19. Heating Data on Centerline of MSL Forebody at 16^O Angle of Attack for Run 5 (10 MJ/kg run condition)

is likely to be laminar. The fact that it under-predicts farther down the body is a result of the transitional behavior of the flow. This observation is consistent with the observation made with the hemisphere model during the calibration phase that was shown in Fig. 8. Unlike the 5 MJ/kg conditions, the catalytic behavior of the flow seems to be limited in some way, although the effect seems to be less pronounced on the MSL than it was for the hemisphere. One reason this could be is that the MSL is an order of magnitude larger than the hemisphere, which may impact the dimensionless scale of the surface reaction rates. Also, the peak level is much smaller on the MSL than it was on the hemisphere model, so the effect may seem to be more dramatic visually when looking at the hemisphere plot. The fact that the data for run 5 shows about 90% of the super-catalytic heating level in the nose explains why it did not look notably different in the scatter of the non-dimensional points of the runs in Fig. 16.

VI. Conclusion

Laminar and turbulent data was obtained on a 61cm (24") diameter MSL model in the LENS-I facility. This data was obtained at angles of attack of 0^O, 11^O, and 16^O. The large physical size of the model provided transition data for all three configurations, despite early estimations that turbulent data would only be possible at the largest angle of attack. At all three angles of attack, the data on the leeward side of the model behaved as expected, with the runs at the largest Reynolds numbers transitioning sooner than those at smaller Reynolds numbers. Analysis of this data was used to generate transition criteria for the leeward side of the model.

Several outstanding issues remain to be fully explained at the conclusion of the MSL program. First is the issue of potential transitional behavior on the windward side of the model. The large size of the model may provide some justification for this behavior. The fact that symmetric measurements were found at 0^O angle of attack demonstrates that there was no systematic problem with the facility, the model, or the instrumentation. This effect will be studied more fully with a smaller scale model as part of future work in the LENS-I facility.

The second major issue is that of the catalytic behavior of the model. A mechanism was found and proposed for the consistent catalytic heating enhancement on the model. Additionally, this catalytic phenomenon seems to be independent of the type of heat transfer instrumentation used, and a similar behavior was reported in the T5 tests. The magnesium fluoride coating applied to the model was apparently totally ineffective in reducing the catalytic heating, although the reason for this is not understood. One of the most plausible explanations is that the coating was quickly worn off the model, but this presumption has not been validated. The rate of the catalytic reactions seem to be such that they go to completion at the 5 MJ/kg cases, while there is some evidence that they may be rate limited at the higher 10 MJ/kg conditions. More investigation is required to fully understand these mechanisms.

We have demonstrated the capability to test in carbon dioxide with the LENS-I facility to support current and future missions to Mars. The large physical size and long run times of the facility provide the capability to study essential effects like turbulent transition and wake flow to design Martian reentry bodies. The remaining issues from the program that have been discussed here are priority items for future work in this area.

Acknowledgments

This work was performed under contract with NASA Langley Research Center.

References

[1]Park, C.; Howe, J.T.; Jaffe, R.J.; and Candler, G.V. "Review of Chemical-Kinetic Problems of Future NASA Missions II: Mars Entries". *Journal of Thermophysics and Heat Transfer*. Vol 8, no 1. Pgs 9 – 23. 1994.

[2]Hollis, B.R.; Liechty, D.S.; Wright, M.W.; Holden, M.S.; Wadhams, T.P.; MacLean, M.; and Dyakonov, A. "Transition Onset and Turbulent Heating Measurements for the Mars Science Laboratory Entry Vehicle". AIAA Paper 2005-1437. 43^{RD} Aerospace Sciences Meeting & Exhibit. Reno, NV: 10-14 January 2005.

[3]Wright, M.J.; Olejniczak, J.; Brown, J.L; Hornung, H.G.; and Edquist, K.T. "Computational Modeling of T5 Laminar and Turbulent Heating Data on Blunt Cones, Part 2: Mars Applications". AIAA Paper 2005-0177. 43^{RD} Aerospace Sciences Meeting & Exhibit. Reno, NV: 10-14 January 2005.

[4]Lu, F.K. and Marren, D.E. Eds. *Advanced Hypersonic Test Facilities*. AIAA Progress in Astronautics and Aeronautics Series: Vol 198. Chapter 4. Reston, VA: American Institute of Aeronautics and Astronautics, 2002.

[5]Holden, M.S.; Wadhams, T.P.; and Candler, G.V. "Experimental Studies in the LENS Shock Tunnel and Expansion Tunnel to Examine Real-Gas Effects in Hypervelocity Flows". AIAA Paper 2004-0916. January 2004.

[6]MacLean, M.; Candler, G.; and Holden, M. "Numerical Evaluation of Flow Conditions in the LENS Reflected Shock-Tunnel Facilities". AIAA Paper 2005-0903. 43^{RD} Aerospace Sciences Meeting & Exhibit. Reno, NV: 10-14 January 2005.

[7]Gaydon, A.G. and Hurle, I.R. *The Shock Tube in High-Temperature Chemical Physics*. New York: Reinhold Publishing Co., 1963.

[8]Lordi, J.A. and Mates, R.E. *Non-equilibrium Expansions of High-Enthalpy Airflows*. Cornell Aeronautical Laboratory Report, ARL 64-206. November 1964.

[9]Eggers, A.J. Jr. *One-dimensional Flows of an Imperfect Diatomic Gas*. NACA TR-959. Moffett Field, CA: Ames Aeronautical Laboratory, 30 Dec 1948.

[10]Korte, J.J.; Hedlund, E.; and Anandakrishnan, S. "A Comparison of Experimental Data With CFD For The NSWC Hypervelocity Wind Tunnel #9 Mach 14 Nozzle". AIAA Paper 92-4010. 17TH Aerospace Ground Testing Conference. Nashville, TN: 6-8 July 1992.

[11]Candler, G. "Hypersonic Nozzle Analysis Using an Excluded Volume Equation of State". AIAA Paper 2005-5202. 38TH Thermophysics Conference. Toronto, Canada: 6-9 June 2005.

[12]Moran, M.J. and Shapiro, H.N. *Fundamentals of Engineering Thermodynamics*, 2ND Ed. New York: John Wiley & Sons, Inc. ISBN 0-471-53984-8. 1992.

[13]McBride, B.; Zehe, M.; and Gordon, S. *NASA Glenn Coefficients for Calculating Thermodynamic Properties of Individual Species*. NASA/TP-2002-211556. September 2002.

[14]Wright, M.J.; Bose, D.; and Candler, G.V. "A Data Parallel Line Relaxation Method for the Navier-Stokes Equations". *AIAA Journal*. Vol 36, no 9. Pgs 1603 – 1609. Sept 1998.

[15]MacCormack, R.W. and Candler, G.V. "The Solution of the Navier-Stokes Equations Using Gauss-Seidel Line Relaxation". *Computers and Fluids*. Vol 17, No 1. Pgs 135 – 150. 1989.

[16]Spalart, P.R. and Allmaras S.R. "A One-Equation Turbulence Model for Aerodynamic Flows". AIAA 92-0439. 30TH Aerospace Sciences Meeting & Exhibit. Reno, NV: 6-9 Jan, 1992.

[17]Catris S. and Aupoix B. "Improved Turbulence Models for Compressible Boundary Layers." AIAA 98-2696. 2ND Theoretical Fluid Mechanics Meeting: Albuquerque, NM, June 1998.

[18]Candler, G.V. "Chemistry of External Flows". *Aerothermochemistry for Hypersonic Technology*: Von Karman Institute for Fluid Dynamics Lecture Series. VKI LS 1995-04.

[19]Landau, L. and Teller, E. "Theory of Sound Dispersion". *Physikalische Zeitschrift der Sowjetunion*. Vol 10, no 34. 1936.

[20]Millikan, R. and White, D. "Systematics of Vibrational Relaxation". *Journal of Chemical Physics*. Vol 39, no 12. Pgs 3209 – 3213. 1963.

[21]Camac, M. "CO_2 Relaxation Processes in Shock Waves". *Fundamental Phenomena in Hypersonic Flow*. J.G. Hall Ed. Cornell University Press. Pgs 195 – 215, 1964.

[22]Palmer, G.E. and Wright, M.J. "A Comparison of Methods to Compute High Temperature Gas Viscosity". *Journal of Thermophysics and Heat Transfer*. Vol 17, no 2. Pgs 232 – 239. 2003.

[23]Palmer, G.E. and Wright, M.J. "A Comparison of Methods to Compute High Temperature Gas Thermal Conductivity". AIAA Paper 2003-3913. Jun 2003.

[24]Gupta, R.; Yos, J.; Thompson, R.; and Lee, K. "A Review of Reaction Rates and Thermodynamic and Transport Properties for an 11-Species Air Model for Chemical and Thermal Nonequilibrium Calculations to 30000 K". NASA RP-1232. August 1990.

[25]Ramshaw, J.D. "Self-consistent Effective Binary Diffusion in Multicomponent Gas Mixtures". *Journal of Non-Equilibrium Thermodynamics*. Vol 15, no 3. Pgs 295 – 300. 1990.

[26]Baldwin, B.S. and Lomax, H. "Thin Layer Approximation and Algebraic Model for Separated Turbulent Flows". AIAA Paper 78-0257. Huntsville, AL: 1978.

[27]Menter, F.R. "Two-Equation Eddy-Viscosity Turbulence Models for Engineering Applications". *AIAA Journal*. Vol 32, no 8. Pgs 1598 – 1605. August 1994.

[28]Brown, James. "Turbulence Model Validation for Hypersonic Flow". AIAA Paper 2002-3308. 8TH Thermophysics and Heat Transfer Conference. St. Paul, MN: 24 – 26 Jun 2002.

[29]Mitcheltree, R. and Gnoffo, P. "Wake Flow About a MESUR Mars Entry Vehicle". AIAA Paper 94-1958. 1994.

[30]Bonzel, H.P. and Ku, R. "Carbon Monoxide Oxidation on a Pt(110) Single Crystal Surface". *The Journal of Vacuum Science and Technology*. Vol 9, no 2. Pgs 663 – 667. 1972.

[31]Hiratsuka, K.; Kajdas, C.; and Yoshida, M. "Tribo-Catalysis in the Synthesis Reaction of Carbon Dioxide". *Tribology Transactions*. Vol 47. Pgs 86 – 93. 2004.

[32]Stampfl, C. and Scheffler, M. "Mechanism of Efficient Carbon Monoxide Oxidation at Ru(0001)". *Journal of Vacuum Science and Technology A*. Vol 15, no 3. Pgs 1635 – 1641. May/June 1997.

[33]Jenkins, D.R. and Voisey, M.A. "The Catalytic Reduction of Nitric Oxide in Automobile Exhaust Gases-II. The Kinetics of the Reactions of Carbon Monoxide with Nitric Oxide and/or Oxygen on an Oxidized Stainless-Steel Surface". *Atmospheric Environment*. Vol 7, no 2. Pgs 187 – 199. Feb 1973.

[34]Williams, R. "Application of Pulse Facilities to Inlet Testing". *Journal of Aircraft*. Vol 1, no 5. Pgs 236 – 241. Sept-Oct 1964.

[35]Olejniczak, J.; Wright, M.J.; Brown, J.L.; and Hornung, H. "Computational Modeling of T5 Laminar and Turbulent Heating Data on Blunt Cones, Part 1: Titan Applications". AIAA Paper 2005-0176. 43RD Aerospace Sciences Meeting & Exhibit. Reno, NV: 10-14 January 2005.